Check for updates

Early treatment with anti-$\alpha_4\beta_7$ antibody facilitates increased gut macrophage maturity in SIV-infected rhesus macaques

Samuel D. Johnson[1,2], Lindsey A. Knight[2], Narendra Kumar[2], Omalla A. Olwenyi[1,2], Michellie Thurman[2], Smriti Mehra[3], Mahesh Mohan[3] and Siddappa N. Byrareddy[2,4,5]*

[1]Department of Pathology and Microbiology, University of Nebraska Medical Center, Omaha, NE, United States, [2]Department of Pharmacology and Experimental Neuroscience, University of Nebraska Medical Center, Omaha, NE, United States, [3]Southwest National Primate Research Center, Texas Biomedical Research Institute, San Antonio, TX, United States, [4]Department of Genetics, Cell Biology and Anatomy, University of Nebraska Medical Center, Omaha, NE, United States, [5]Department of Biochemistry and Molecular Biology, University of Nebraska Medical Center, Omaha, NE, United States

Despite advances in combination antiretroviral therapy (cART), people living with HIV (PLWH) continue to experience gastrointestinal dysfunction. Infusions of anti-$\alpha_4\beta_7$ monoclonal antibodies (mAbs) have been proposed to increase virologic control during simian immunodeficiency virus (SIV) infection in macaques with mixed results. Recent evidences suggested that therapeutic efficacy of vedolizumab (a humanized anti-$\alpha_4\beta_7$ mAb), during inflammatory bowel diseases depends on microbiome composition, myeloid cell differentiation, and macrophage phenotype. We tested this hypothesis in SIV-infected, anti-$\alpha_4\beta_7$ mAb-treated macaques and provide flow cytometric and microscopic evidence that anti-$\alpha_4\beta_7$ administered to SIV-infected macaques increases the maturity of macrophage phenotypes typically lost in the small intestines during SIV disease progression. Further, this increase in mature macrophage phenotype was associated with tissue viral loads. These phenotypes were also associated with dysbiosis markers in the gut previously identified as predictors of HIV replication and immune activation in PLWH. These findings provide a novel model of anti-$\alpha_4\beta_7$ efficacy offering new avenues for targeting pathogenic mucosal immune response during HIV/SIV infection.

KEYWORDS

simian immunodeficiency virus (SIV), $\alpha_4\beta_7$ integrin, microbiome, butyrate, myeloid cells, macrophage maturation, mucosal immunology, viral reservoir

Introduction

Human immunodeficiency virus (HIV) infections are associated with significant disruption to gut integrity, including microbial dysbiosis, barrier dysfunction, and resultant chronic immune activation (1, 2). These gut pathologies are similar to the symptomology of inflammatory bowel diseases (IBDs), such as Crohn's disease (CD) and ulcerative colitis (UC), during which abdominal pain, diarrhea, constipation, fatigue, and mood disturbances are commonly reported (3, 4). Currently, vedolizumab, a humanized anti-$\alpha_4\beta_7$ integrin monoclonal antibody (mAb) is effectively used to ameliorate IBD symptoms and reduce associated damage by blocking gut homing of inflammatory cells by antagonizing $\alpha_4\beta_7$ integrin binding to its cognate ligand mucosal addressin cell adhesion molecule 1 (MAdCAM-1) on intestinal endothelium (5). Additionally, differences in $\alpha_4\beta_7$ integrin surface expression on circulating immune cells have been demonstrated between disease-resistant natural primate hosts of the simian immunodeficiency virus (SIV) that do not progress to AIDS-like disease and non-natural hosts that do progress, often to fatal disease, with the latter having significantly higher mean $\alpha_4\beta_7$ integrin surface expression (6).

Recently, a primatized anti-$\alpha_4\beta_7$ mAb reagent was developed that could be repeatedly administered *in vivo* to block the higher levels of $\alpha_4\beta_7$ integrin expression in disease-progressing rhesus macaques (RMs) (7). Furthermore, anti-$\alpha_4\beta_7$ mAb was shown to reduce gut viral loads following SIV infection (8, 9). Similarly, anti-$\alpha_4\beta_7$ therapy was found to reduce gut lymphoid aggregates that could serve as potential HIV-1 reservoirs (10). Despite this reduction, other studies have reported conflicting results suggesting that anti-$\alpha_4\beta_7$ therapy does not reduce peripheral viral loads/viral reservoirs in SIV-infected rhesus macaques (11–13). Intriguingly, in a clinical trial involving the administration of anti-$\alpha_4\beta_7$ mAb to HIV-infected individuals revealed that five out of eighteen participants controlled viremia to less than 1,000 copies per mL for the 26 week duration of analytical antiretroviral therapy interruption highlighting the potential utility of anti-$\alpha_4\beta_7$ therapy towards HIV control (14). Likewise, recent findings noted that anti-HIV broadly neutralizing antibodies-treated RMs that were given anti-$\alpha_4\beta_7$ therapy delayed viral rebound compared to those treated with broadly neutralizing antibodies alone (15). Because some studies have demonstrated benefits, understanding why certain individuals/macaques fail or succeed in controlling viremia following treatment interruption could provide crucial insights into future designs of HIV/SIV cure studies.

Although vedolizumab was initially developed to reduce pro-inflammatory lymphocyte trafficking to the gut, thereby reducing local tissue damage, several studies have questioned this proposed mechanism (16). Compared to infliximab (anti-TNF-α mAb), vedolizumab is not associated with changes to total, CD4+, CD8+, central memory, or effector memory lamina propria T cells in rectal biopsies of CD and UC patients at week 14, following three mAb infusions (17). Even though infliximab was associated with decreased T-cell recruitment to the gut, it was less efficacious than vedolizumab in measures of both clinical response and remission (17). However, vedolizumab was associated with a decrease in pro-inflammatory M1 and an increase in anti-inflammatory M2 macrophages. These changes were predictive of remission (17). Interestingly, macrophage turnover in the intestines is predictive of accelerated disease progression in SIV-infected macaques (18, 19). Whether the similarities between IBD and HIV/SIV pathogenesis include macrophage recruitment remains poorly characterized.

In addition to the emerging understanding of myeloid cells as potential mediators of IBD, new studies involving the role of the microbiome are providing further insights into IBD pathogenesis. Individuals with IBDs tend to have a decrease in markers of overall microbiome richness, including α-diversity measuring total operational taxonomic units (OTUs) and Shannon diversity index, which incorporates weighting species abundance evenness (20, 21). Additionally, IBD is associated with an increase in the ratio of Bacteroidetes: Firmicutes (B: F), including reductions in Firmicute butyrate-producing bacteria (BPB) like *Roseburia* and *Faecelibacterium* (22–24). Similarly, HIV infection is also associated with dysbiosis with an expansion of the Bacteroidetes genus *Prevotella* and a decrease in BPB (25, 26). The relative abundance of BPB in people living with HIV has been inversely correlated with markers of microbial translocation, immune activation, and vascular inflammation (25). These findings raise the question of whether microbiome composition could further modulate anti-$\alpha_4\beta_7$ efficacy in SIV infection, possibly contributing to divergent outcomes during therapy.

We characterized gut macrophage maturation dynamics in the duodenum and ascending colon of SIV-infected RMs utilizing both flow cytometry and microscopy techniques and determined tissue viral loads in each compartment prior to and following anti-$\alpha_4\beta_7$ administration. Additionally, we performed 16S rRNA gene sequencing to determine if microbiome composition impacted these immune dynamics. All macaques were infected with SIVmac251 and CD8-depleted to accelerate pathogenesis as part of a more extensive separate study. As expected, without CD8$^+$ cells, the RMs did not control viral replication, reinforcing recent reports that when CD8+ cells are depleted, anti-$\alpha_4\beta_7$ therapy fails at maintaining viral control during SIV-nef-stop infection (27). However, despite these changes, significant decreases in myeloid cell turnover were seen in the small intestine in the anti-$\alpha_4\beta_7$ group compared to IgG-treated controls. These changes were associated with alterations in tissue viral loads and markers of dysbiosis in the fecal microbiome, suggesting that myeloid cell dynamics and microbiome composition may be crucial to the efficacy of anti-

$\alpha_4\beta_7$ mAb treatment during SIV infection. These findings provide a new variable for differential experimental outcomes that has until now remained undefined.

Materials and methods

Animals and ethics statement

A total of nine outbred Indian-origin rhesus macaques (*Macaca mulatta*) (RMs) with a mean age of 6.1 years old (5.1 to 10.0) were procured from the Yerkes National Primate Center of Emory University, Atlanta, Georgia, the USA and the New Iberia Research Center of University of Louisiana, Lafayette, Louisiana, USA and used in this study as summarized in Table S1. All RMs were housed at the Department of Comparative Medicine, University of Nebraska Medical Center (UNMC), Omaha, Nebraska, the USA, in compliance with regulations outlined in the Animal Welfare Act and the Guide for the Care and Use of Laboratory Animals. Animals were pair-housed with visual access to other monkeys in a temperature-controlled (72°F) indoor climate with a 12-hour light/dark cycle. Animals were fed a monkey diet (Purina) twice daily, supplemented with fresh fruits and water being available *ad libitum*. Animals were anesthetized (ketamine 10 mg/kg or telazol 4 mg/kg) prior to all procedures, and meloxicam (0.2 mg/kg) was administered when appropriate. At the end of the study, euthanasia was performed following the guidelines of the American Veterinary Medical Association by a high dose of ketamine-xylazine followed by exsanguination and cardiac perfusion. This study was approved by the UNMC Institutional Animal Care and Use Committee (IACUC) and the Institutional Biosafety Committee (IBC) under protocol #15-102-12-FC entitled "Gut Trafficking Cells in SIV Infection".

Study design

Nine RMs were randomly divided into two groups: four in the control group were administered control IgG and five in the experimental group treated with a primatized monoclonal anti-$\alpha_4\beta_7$ IgG. All monkeys were depleted of CD8+ cells by the administration of a rhesus recombinant IgG1 anti-CD8α mAb (MT807R1) Lot: 100LBRX-3206-023-001 (NIH Nonhuman Primate Reagent Resource) four times spanning several days before and after infection (Day -4: 10 mg/kg subcutaneously and on days -1, 3, and 6 administered 5 mg/kg intravenously). On Day 0, all macaques were intravenously inoculated with 1000 TCID$_{50}$ SIVmac251 (Source: Simian Vaccine Evaluation Unit, NIAID, NIH). During acute infection on Day 12, daily intramuscular administration of a combination of anti-retroviral therapy (cART) (20 mg/kg TFV + 40 mg/kg FTC + 2.5 mg/kg DTG) was initiated and continued until Week 14. On day 15, while the controls were administered 50 mg/kg rhesus IgG1 control antibody rhesus IgG1

mAb (DSPR1) Lot: LH15-35 (NIH Nonhuman Primate Reagent Resource), the experimental group monkeys were administered 50 mg/kg rhesus recombinant IgG1 anti-$\alpha_4\beta_7$ mAb (A4B7, Lot: LH17-14-NIH Nonhuman Primate Reagent Resource). Antibody infusions were continued every three weeks until week 23 for a total of eight infusions. Blood was collected from the saphenous vein using K2-EDTA vacutainer tubes (Becton, Dickinson, San Diego, CA, USA) for monitoring plasma viral loads. Feces were collected using fecal loops at baseline and on days 14, 98, and 161 and were snap frozen for future analysis. At necropsy, gut tissues were collected, a portion snap frozen, a portion fixed in 10% formalin, and additional tissue used for immune cell isolation (below) for flow cytometry. An illustration of the study design is available in Figure S1.

Intestinal cell isolation

At necropsy, duodenum and ascending colon were collected, washed with DPBS, and dissected into two compartments: 1) epithelium and lamina propria and 2) muscularis externa and serosa. Tissue-specific immune cells were isolated by mincing, digestion with 10,000 U Collagenase, Type 4 (Worthington Biochemical Corporation, Lakewood, NJ, USA; Product #LS004188) and 25 U DNAse I (Roche Diagnostics, Mannheim, Germany; Product #LS004188) in 10 mL DPBS for two hours, filtration through 100 µm and 40 µm sterile cell strainers (Fisherbrand, Hampton, NH, USA; Product #22-363-549 and 22-363-547), and density gradient centrifugation with 60% and 30% Percoll (Cytiva, Uppsala, Sweden; Product #17089101) layers at 2000 rpm for 30 minutes. Isolated cells were washed with DPBS and resuspended in RPMI.

Flow cytometry

Isolated gut cells were sequentially incubated with Zombie Aqua Fixable Viability Dye (BioLegend, San Diego, CA, USA; Product #423102) to discriminate live/dead cells and incubated with Fc blocker to minimize non-specific binding and then stained with a panel of fluorescent-dye conjugated antibodies (Table S2), and then fixed with 1% PFA. Both compensation and fluorescent minus one (FMO) controls were utilized to assist in gating placement. Event acquisition was performed using a Fortessa x450 flow cytometer (B-D, Mountain View, CA). Analysis was performed with FlowJo 10.6.1 software (Treeland, OR). To determine macrophage maturity, a gating strategy developed by Bujko, et al. was utilized (see Figure S2) (28).

Viral loads

Viral loads were determined as has been described previously (29). In brief, plasma was separated from whole

blood by centrifugation at 1200 rpm for 20 minutes, and RNA was isolated using a QIAamp viral RNA Mini Kit (Qiagen, Germantown, MD, USA; Product #52906). Frozen gut tissue was lysed using a TissueLyser LT (Qiagen, Germantown, MD, USA; Product #69980), and then DNA and RNA were isolated using an AllPrep DNA/RNA Mini Kit (Qiagen, Germantown, MD, USA; Product #80204) according to manufacturer instructions. Copies of SIVgag DNA were normalized to cell number by quantifying genomic RPP30 as previously described to determine copies/cell (30).

16S rRNA sequencing

Fecal samples were later thawed and approximately 100-200 mg of fecal sample was used to isolate DNA using spin column chromatography-based Stool DNA Isolation Kit (Norgen Biotek Corp; Product #27,600) following manufacturer recommendations. DNA was quantified with a GE SimpliNano spectrophotometer and shipped on dry ice to LC Sciences, LLC (Houston, TX, USA) for 16S rRNA sequencing. A library was generated by amplifying the V3 and V4 16S rRNA variable regions and adding sequencing adapters and barcodes after the first cycle. An Illumina cBot system was used to generate clusters for sequencing with an Illumina MiSeq platform. Barcodes were used to separate data, and an in-house script was used to annotate taxa according to RDP, Greengenes, and NCBI 16SMicrobial customized databases for reference. Data output statistics, including clustering into operational taxonomic units (OTU), diversity analysis, species classification, and abundance analysis were performed by LC Sciences, LLC (Houston, TX). FASTQ files were deposited in the NCBI Sequence Read Archive with the BioProject accession number PRJNA870961.

Immunofluorescence microscopy

Formalin-fixed gut tissues collected at necropsy were embedded in paraffin blocks, cut into 5 μm sections using a microtome (Leica Biosystems, Deer Park, IL, USA; Product #RM2235), and placed on positively charged slides (Avantik, Pine Brook, NJ, USA; Product #SL6332). Tissue sections were deparaffinized with xylene and rehydrated with graded ethanol to water. Antigen retrieval was performed by Decloaking Chamber^{TM} NxGen (Biocare Medical, LLC, Pacheco, CA, USA; Product #DC2012). Tissues were washed three times with water, and a blocking buffer (5% normal goat serum + 1% BSA in PBS) was applied for one hour at room temperature to prevent non-specific binding. Sections were incubated overnight with anti-CD163 and anti-CD206 antibodies (Table S3) at 4°C. Tissues were washed with PBS and incubated for one hour with fluorescent secondary antibodies (Table S3) at room temperature. Tissues were finally washed five times with PBS,

Prolong^{TM} Gold antifade reagent with DAPI (Invitrogen Waltham, MA, USA; Product #P36935) was added, and coverslips were applied. 20X images were captured using a LIONHEART LX Automated Microscope (BioTek, Santa Clara, CA) using Gen5 3.05 software. Co-localization was performed using the JAKoP plug-in for Image J 1.53e (31).

Statistical analysis

Mann-Whitney tests were implemented when comparing data obtained on the anti-$\alpha_4\beta_7$ with those obtained on the control groups. Multiple t-tests were utilized when comparing myeloid cell phenotypes. Two-way ANOVA, linear regression, and ratio paired T-tests were performed as specified. All statistical analysis was performed with GraphPad Prism 7 for Mac OS X. Statistical significance was determined as $P \leq 0.05$.

Results

Anti-$\alpha_4\beta_7$ therapy is associated with increased macrophage maturity in the duodenum

Contrary to early reports, more recent data has increasingly suggested that the mechanism of action for anti-$\alpha_4\beta_7$ mAbs is more complex than blocking inflammatory lymphocyte infiltration (16). These studies have indicated that myeloid cells, particularly macrophages and DCs, may contribute to the efficacy of vedolizumab (17, 32, 33). To characterize changes in gut myeloid cell differentiation at necropsy, immune cells were isolated from the lamina propria and muscularis externa of the duodenum and ascending colon. The isolated cells were subjected to flow cytometry and a gating strategy was utilized based on a previously described method developed by Bujko, et al., (Figure S2) which was focused on the characterization of gut myeloid cells across developmental stages from monocyte-like macrophages (Mf1), intermediate macrophages (Mf2), to mature (Mf3) macrophages (28). Additionally, this strategy identifies muscularis macrophages (Mf4), determining their frequency as a percent of total macrophages.

Compared to the mean frequency of 63.0% Mf1 macrophages in the duodenum lamina propria of the control group, as seen in Figure 1A, the anti-$\alpha_4\beta_7$ treated group showed a significant reduction (mean 14.6%) (P=0.01). Similarly, there was a trend in reduction of Mf2s in the same tissues with mean values of 16.1% in the control and 3.8% in the anti-$\alpha_4\beta_7$ mAb treated group (NS) (Figure 1A). In contrast, anti-$\alpha_4\beta_7$-treated RMs had higher mean frequencies of the Mf3 macrophages (63.9%) than 20.4% in the control group (P=0.02). Similarly, there was a trend in increased Mf4s with anti-$\alpha_4\beta_7$-treatment (17.7% compared to 0.6%, NS), a minority population in the

duodenum lamina propria. Similarly, although statistically non-significant, there was a trend in reduced Mf2s and increased Mf3s in the duodenum muscularis externa in the control group as compared to the anti-$\alpha_4\beta_7$-treatment group.

As mentioned, Bujko, et al. developed a gating strategy for analyzing cells isolated from the small intestine (28). We applied this strategy to cells isolated from the ascending colon (28). No significant differences were found in any of the macrophage subtypes in either the lamina propria or muscularis externa Figure 1B. Despite this, some trends existed between the small

and large intestinal macrophage subtypes. In all tissue samples, intermediate Mf2s were lower with anti-$\alpha_4\beta_7$ treatment and, when combined, were significantly different with a mean of 6.5% compared to 26.2% with values from the IgG treatment group (P=0.02). Conversely, in most samples, Mf4s were higher with anti-$\alpha_4\beta_7$ treatment. Combined, the anti-$\alpha_4\beta_7$-treatment group had a mean of 15.1% Mf4s compared to 5.8% in the control group (P=0.03). As expected, there was a trend in higher Mf1s and Mf3s in the lamina propria and Mf4s in the muscularis externa.
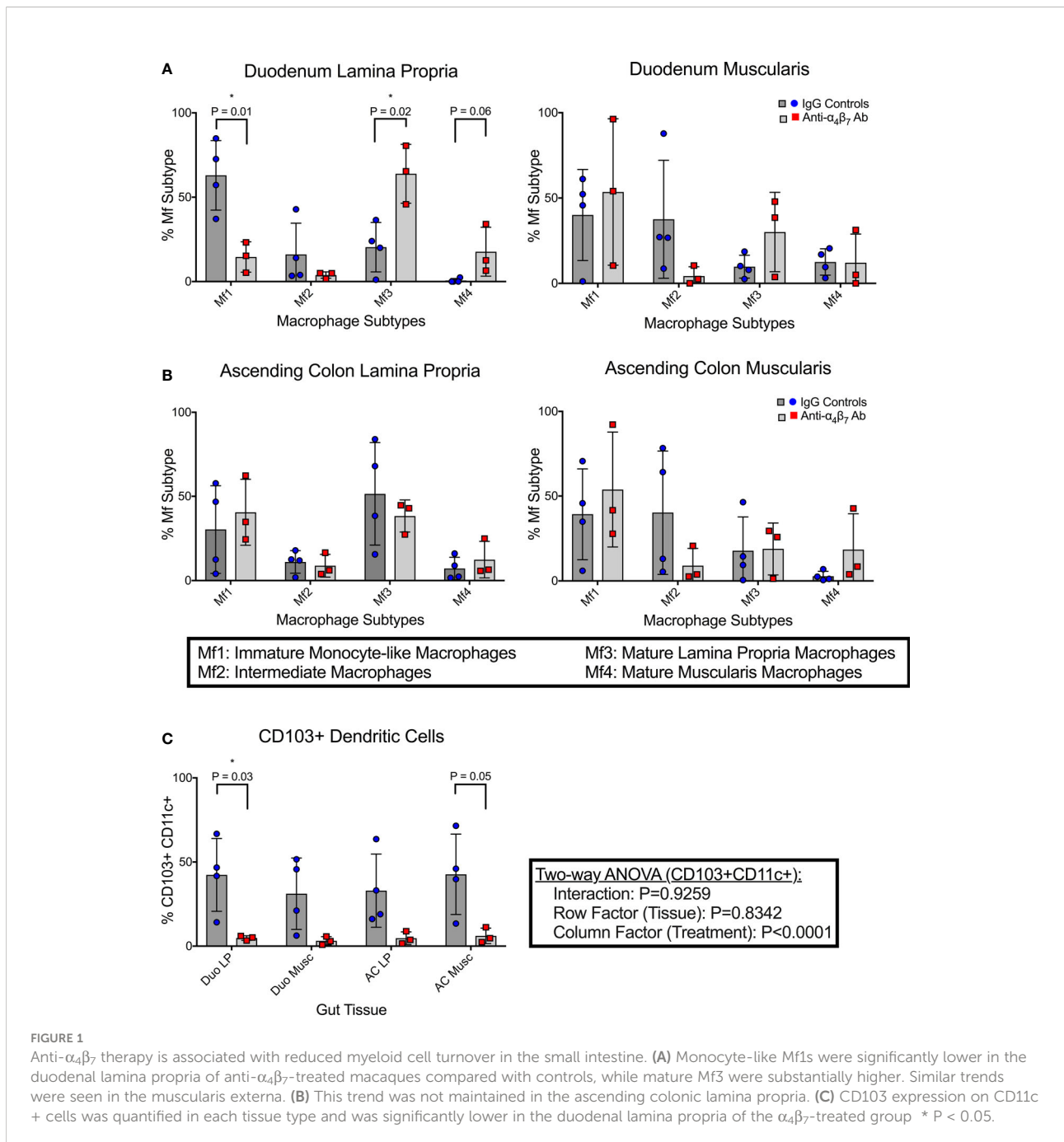
FIGURE 1

Anti-$\alpha_4\beta_7$ therapy is associated with reduced myeloid cell turnover in the small intestine. **(A)** Monocyte-like Mf1s were significantly lower in the duodenal lamina propria of anti-$\alpha_4\beta_7$-treated macaques compared with controls, while mature Mf3 were substantially higher. Similar trends were seen in the muscularis externa. **(B)** This trend was not maintained in the ascending colonic lamina propria. **(C)** CD103 expression on CD11c + cells was quantified in each tissue type and was significantly lower in the duodenal lamina propria of the $\alpha_4\beta_7$-treated group * P < 0.05.

In addition to pro-inflammatory macrophages, localization of dendritic cells (DCs) to the gut has also been coupled to the expression of the β_7 integrin (33). This includes CD103+ conventional DCs responsible for imprinting lymphocytes with gut-homing function by releasing retinoic acid (33). The frequencies of CD103+ expressing CD11c+ dendritic cells were quantified in each histological layer (lamina propria and muscularis externa) of both the duodenum and colon (Figure 1C). In the duodenum lamina propria, anti-$\alpha_4\beta_7$'s therapy was associated with a significantly lower CD103+ DCs (4.8%) compared to controls (42.4%) (P=0.03). Similar trends were seen in the duodenum muscularis (3.2%, 28.0%; P=0.08), ascending colon lamina propria (4.7%, 33.0%; P=0.08), and ascending colon muscularis (6.1%, 42.7%; P=0.05), with all tissues having lower CD103+ CD11c+ cells in the anti-$\alpha_4\beta_7$ group. A two-way ANOVA analysis was performed to determine whether the response was dependent on tissue type. No significance was found in the tissue (row factor) or interaction, but the treatment (column factor) was significantly different (P<0.0001), suggesting that the differences were due to treatment and not secondary to the tissue being sampled.

Anti-$\alpha_4\beta_7$ therapy is associated with increased colocalization of CD206 with CD163 in gut tissues

Previously, it has been suggested that intestinal macrophage turnover is associated with peripheral monocyte turnover and is predictive of disease progression in SIV-infected RMs (19). To demonstrate these associations, a gating strategy determining the ratio of CD163+CD206+ double-positive to CD163+CD206- single-positive cells was utilized in conjunction with BrdU/EdU-labeling and confocal microscopy, with the finding that disease progression is associated with a reduction in the ratio of double-positive to single-positive cells during SIV infection (19). To validate our flow cytometry findings, we utilized a similar strategy to determine the co-localization of CD206 with CD163 in gut tissues (duodenum and ascending colon) of each of the macaques obtained at necropsy (Figure 2A, C). In addition to providing further evidence for increased macrophage maturity utilizing different surface markers (Bujko's strategy does not include either CD163 or CD206), this strategy also provided data for the two anti-$\alpha_4\beta_7$-treated RMs with missing flow cytometry data (19). When co-localization of CD206 with CD163 was measured in the duodenum, Mander's coefficient 1 (MC1) was measured providing the ratio of co-localization compared with total CD163 expression. In the IgG-treated controls, the mean MC1 was 0.07 compared with 0.53 in the anti-$\alpha_4\beta_7$-treated group (P=0.0159) (Figure 2B). When the same strategy was performed for the ascending colon, while the control group was 0.35, the anti-$\alpha_4\beta_7$-treated group was 0.53 (P=0.0397) (Figure 2D). In each tissue, the lower MC1 in the

control group suggests reduced macrophage maturity compared with the experimental group.

These readings were next compared with macrophage subtype in the duodenum, as expected, Mf1s were negatively associated with MC1 (r=-0.8523, P=0.0148), and Mf3s (r=0.7706, P=0.0426) and Mf4s (r=0.777, P=0.0398) were positively associated with MC1 (Figure 2E). While there was a trend in a negative association with Mf2s, this correlation was not significant. This finding is consistent with Bujko, et al's decision to not use CD206 as a marker for their gating strategy because CD206 is expressed at high levels on Mf2, Mf3, and Mf4 gut macrophages (28).

Anti-$\alpha_4\beta_7$ therapy is associated with changes in tissue viral loads

There were no statistical differences between plasma viral loads during the post-treatment interruption between treated and control animals (Figure S6). However, we found significantly higher DNA viral load in the duodenum of anti-$\alpha_4\beta_7$-treated macaques (geometric mean: 536 copies/10^6 cells) compared to controls (geometric means 106 copies/10^6 cells; P=0.02) as determined by copies of SIVgag compared to the host genomic gene RPP30 (Figure 3A). No difference in DNA viral loads was found in the ascending colon (387 versus 382 copies/10^6 cells). A similar trend was seen in RNA viral loads, with the duodenum of the anti-$\alpha_4\beta_7$ group having a geometric mean of $\log_{10}$ 5.8 copies/100 ng RNA compared with to $\log_{10}$ 4.0 in controls (Figure 3B). Again, no difference was found in the ascending colon ($\log_{10}$ 5.6 copies compared to $\log_{10}$ 5.8 copies). Next, to determine whether there was a relationship between myeloid cells and viral loads, we performed linear regression analysis on the lamina propria, which were the presumed foci of anti-$\alpha_4\beta_7$ activity. When both experimental design groups are combined for the duodenum, RNA viral loads were negatively correlated with Mf1s (r= -0.8758, P= 0.0098), positively correlated with Mf3s (r= 0.9332, P=0.0021), and negatively correlated with CD103$^+$ DCs (-0.8298, P=0.0209) (Figure 3C). Despite few differences between groups in tissue viral load and macrophage maturity phenotype, the two were similarly correlated in the ascending colonic lamina propria with Mf1s negatively (-0.8366, P=0.0190) and Mf3s positively (r=0.771, P=0.0424) correlated (Figure 3D). CD103$^+$ DCs, though were not significantly associated (r=-0.4899, P=0.2644). Thus, in both the small and large intestines, more mature macrophage phenotypes are associated with viral loads but not necessarily CD103+ DCs. Additionally, the duodenum viral load is associated with MC-1 (r=0.7255, P=0.0270) (Figure S5). However, this Pearson's coefficient is lower than that found when comparing Mf3s (r=0.7255 vs. r=0.9332, respectively), suggesting that fully mature Mf3s, but not all CD163$^+$CD206$^+$ cells, are closely associated with tissue viral loads.
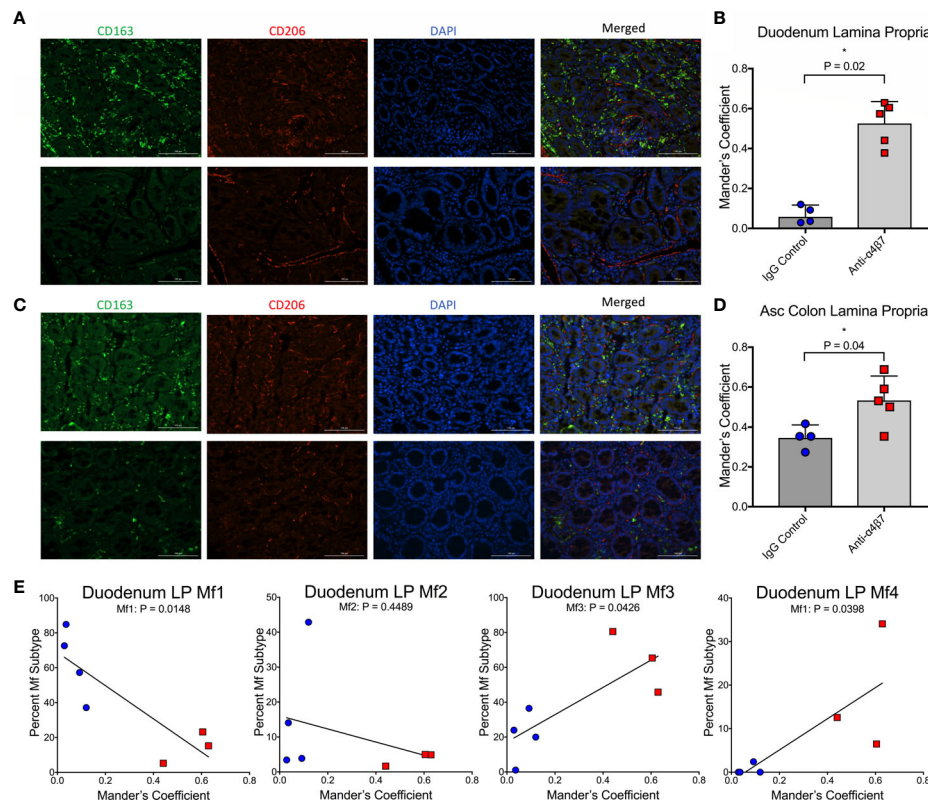
FIGURE 2

Anti-$\alpha_4\beta_7$ therapy is associated with increased CD206+ expression on CD163+ cells. **(A)** Immunofluorescence microscopy was used to compare the expression of CD163 and CD206 in duodenum tissue from anti-$\alpha_4\beta_7$-treated (above) and IgG controls (below). **(B)** Co-localization was quantified with Mander's coefficient 1, showing the ratio of co-localization of CD206 with CD163. **(C)** Immunofluorescence and **(D)** co-localization were also determined for anti-$\alpha_4\beta_7$-treated (above) and IgG controls (below) in the ascending colon. **(E)** Linear regression analysis was used to compare co-localization with duodenal lamina propria macrophage subtypes determined by flow cytometry. * P < 0.05.

Acute SIV infection is associated with acute intestinal dysbiosis

Increasingly, the microbial composition has been recognized as a significant modulator of the inflammatory states of mucosal gut myeloid cells (34). Additionally, specific taxa have been linked with vedolizumab efficacy in IBD patients and lymphocyte activation and viral load during HIV infection (25, 35). To determine whether the microbiome may be influencing the efficacy of anti-$\alpha_4\beta_7$ during SIV infection, 16S rRNA gene sequencing was performed on DNA isolated from fecal samples obtained at baseline, acute infection (Day 14), during therapy (Day 98), and after cART interruption (Day 161). Using unweighted principal component analysis, it was clear that acute infection was associated with dysbiosis, with animals in each group having microbial composition divergence at Day 14 compared with the other timepoints (Figure S3a). Additionally, at the phylum level, non-significant differences were seen in the Bacteroidetes: Firmicutes (B: F) ratio, with the anti-$\alpha_4\beta_7$-treated group experiencing an increase in Bacteroidetes (B) and a

decrease in Firmicutes (F) resulting in an increased B:F ratio at Day 14 (Figure S3c). Control animals had the opposite trend suggesting that each group experienced divergent dysbiosis before therapeutic intervention. It should be noted that in the present study, all RMs were CD8-depleted to facilitate rapid viremia and accelerated pathogenesis. Whether CD8 depletion also modulates microbiome composition in SIV-infected macaques remains to be fully elucidated. However, CD8 depletion prevents respiratory syncytial virus-associated dysbiosis in mice, reversing losses in the Firmicute families Lachnospiraceae and Lactobacillaceae (36).

For greater granularity in taxonomic changes, we next analyzed the family composition of the microbiome over the time course of the experiment. The data was examined using stacked grouped abundance graphs that demonstrated that samples from Day 14 in each group differed from other timepoints with higher Bray-Curtis dissimilarity in both control and experimental groups (Figure 4A). Other time points in each group clustered together with reduced dissimilarity, indicating that each group partially recovered
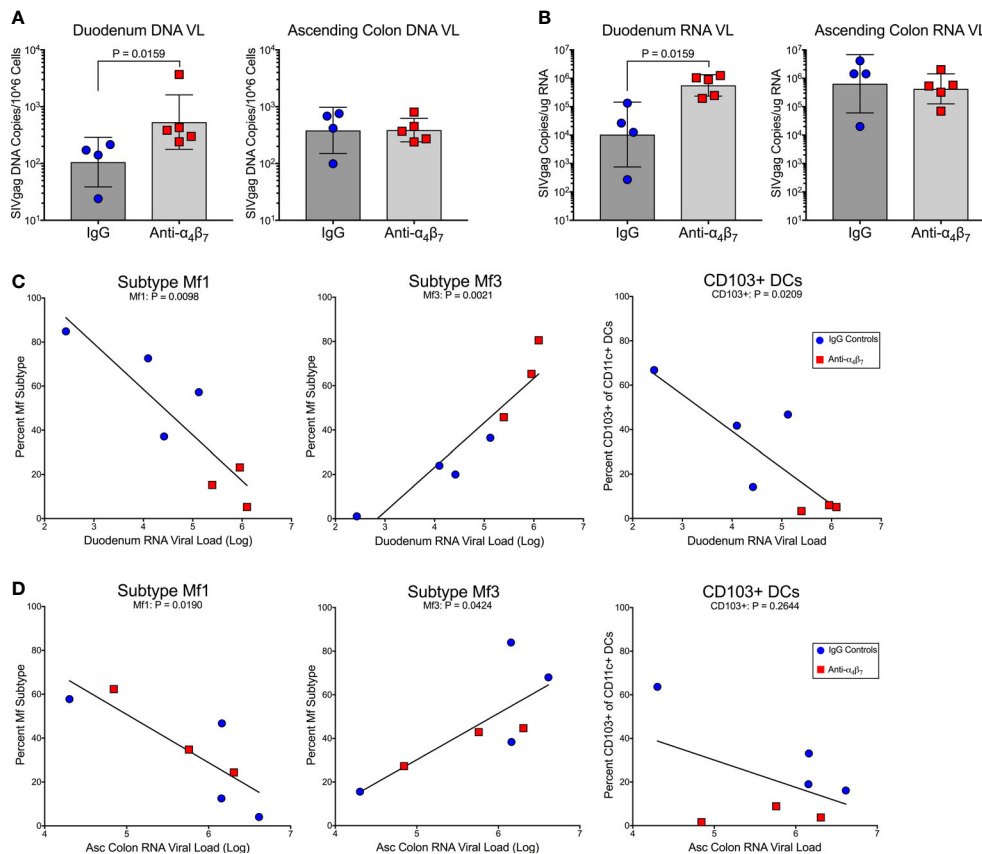
FIGURE 3

Anti-$\alpha_4\beta_7$ therapy was associated with higher small intestine tissue viral loads. **(A)** Tissue RNA viral loads were significantly higher in the duodenum of anti-$\alpha_4\beta_7$-treated macaques compared to controls. **(B)** Tissue DNA viral loads normalized to cell number followed the same trend. **(C)** In the duodenum, viral loads were negatively associated with Mf1s and CD103+ DCs. Viral loads were positively associated with mature Mf3s. **(D)** In the ascending colon, a similar association was found with local viral load and macrophage maturity but not with CD103+ CD11c+ cells.

from acute dysbiosis. A heatmap demonstrates similar dynamics, with data on Day 14 samples considered as outliers in each experimental group (Figure 4B). Critical families from the above analyses were separated to evaluate specific taxonomic changes better, and longitudinal plots were generated (Figure 4C). Prevotellaceae, the most abundant family across all groups, was depleted during acute dysbiosis in the IgG controls, making up only 6.7% in samples from Day 14 compared to 33.3% at baseline. This impact on the relative abundance of Prevotellaceae did not follow a similar trend in the anti-$\alpha_4\beta_7$-treated experimental group. Conversely, Spirochaetaceae were moderately increased in control IgG group from baseline compared to samples on day 14 (7.8% as compared with 17.6%). None of the above differences were statistically significant between groups due to significant inter-individual variations in microbiome composition. However, both groups had an increase in the relative abundance of the family Helicobacteraceae and a decrease in the family

Lactobacillaceae, the latter was significantly different (from 5.8% to 0.3%, P=0.003), with every animal showing a decrease in relative abundance during acute dysbiosis by an average of 88%. Aside from the differences in Prevotellaceae, Lachnospiraceae dynamics were also different between the two groups showing a decrease in the anti-$\alpha_4\beta_7$-treated group (10.2% at baseline to 8.3%) but an increase in the control group (6.6% to 7.6%). A final significant difference between the two groups was seen in the numbers of the Veillonelaceae family, which was significantly depleted (P=0.03) in the IgG-treated controls after infection but rebounded (P=0.03).

SIV-associated dysbiosis is partially ameliorated following anti-$\alpha_4\beta_7$ therapy

HIV/SIV-associated dysbiosis has been extensively characterized across human populations and non-human
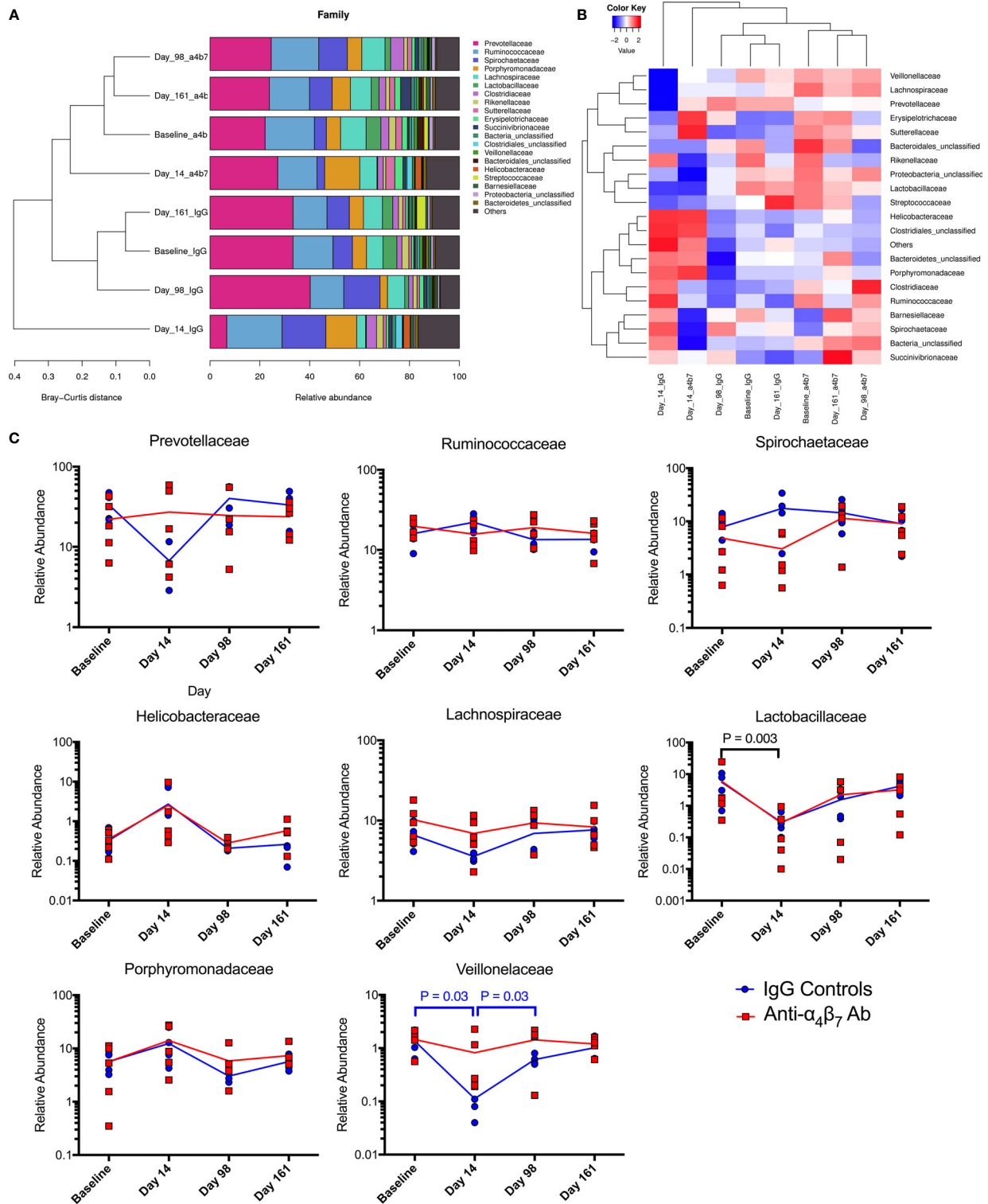
FIGURE 4

Microbiome family composition is disrupted by acute SIV infection: Both **(A)** stacked grouped abundance and **(B)** heatmap demonstrate acute dysbiosis at Day 14 post-infection where family relative abundance does not group within experimental groups. **(C)** Longitudinal changes to family abundance of Prevotellaceae, Ruminococcaceae, Porphyromonadaceae, Spirochaetaceae, Lachnospiraceae, Lactobacillaceae, Helicobacteraceae, and Veillonelaceae.
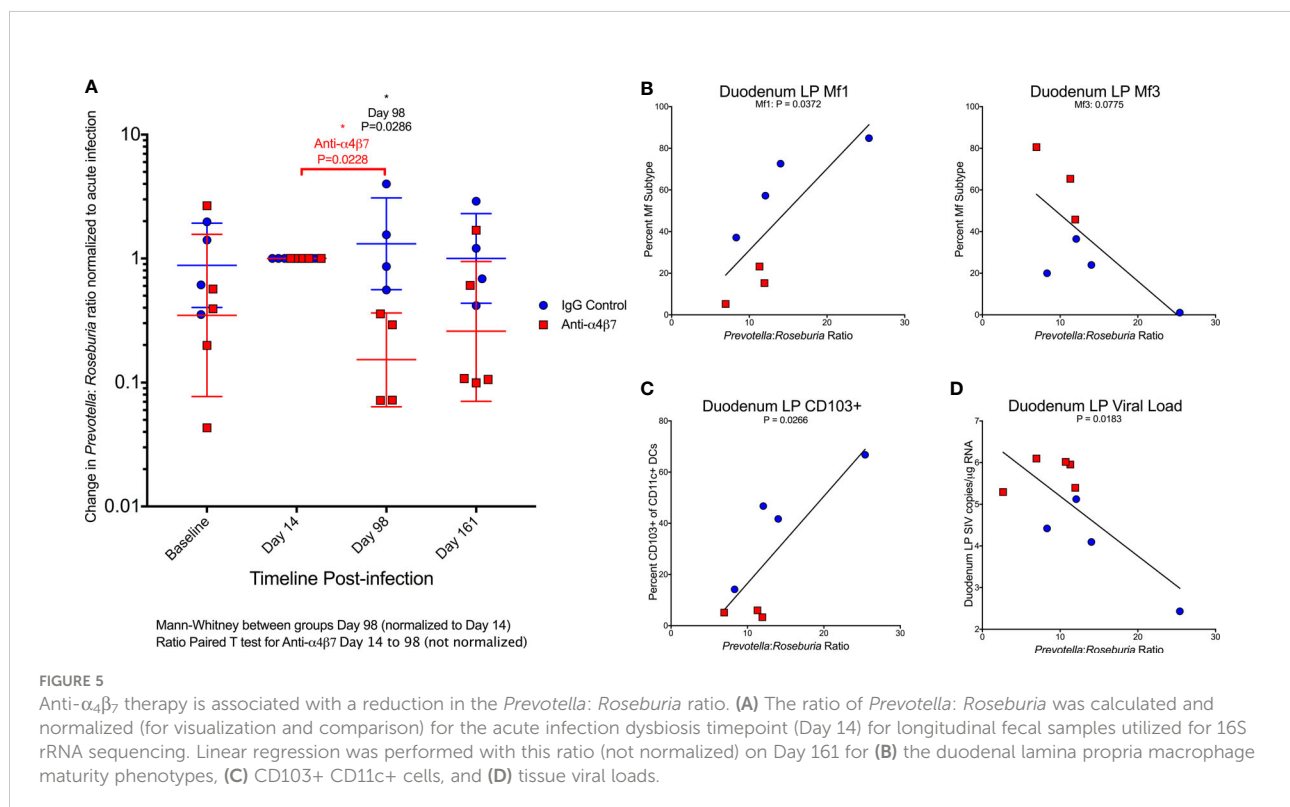
primate models. Consistently, infection is associated with an increase in the Bacteroidete: Firmicute ratio in fecal samples. These changes are primarily driven by increases in *Prevotella* and loss of BPB (25, 26, 37, 38). Notably, the BPB genus *Roseburia* has specifically been linked to vedolizumab efficacy, as a marker of HIV-associated dysbiosis (35). The ratio of these two bacteria groups has previously been used as a marker of dysbiosis during HIV infection, significantly higher in PLWH (25). Further, this ratio was positively associated with lymphocyte and colonic dendritic cell activation (25). As previously noted, there was a divergent dysbiosis prior to infection between the IgG and anti-$\alpha_4\beta_7$ groups. Because of this difference and for improved graphical representation, the *Prevotella*: *Roseburia* ratio was normalized to acute infection (Day 14), the time point at which the microbiome is significantly disrupted and is unable to recover, even with cART (Figure 5A). At acute infection, both groups trend to show an increase in the *Prevotella*: *Roseburia* ratio, regardless of whether normalization was performed, consistent with previous observations of acute infection-associated dysbiosis in both HIV and SIV infections (25, 38, 39). One fecal sample on Day 98 was not collected from the anti-$\alpha_4\beta_7$-treated group. However, in all four animals from which samples were collected, the values were lower following therapy. When normalized to acute infection ratio, a significant difference was found between the IgG- and anti-$\alpha_4\beta_7$-treated groups (P=0.0286). Even without normalization, the change from acute infection to post-treatment *Prevotella*: *Roseburia* ratio was significant in the anti-$\alpha_4\beta_7$-treated group

compared using a ratio paired T-test that showed a decrease from a geometric mean of 29.7 to 6.5 (P=0.0228).

When the Day 161 *Prevotella*: *Roseburia* ratio was compared with macrophage turnover in the duodenal lamina propria, Mf1s were positively associated (r=0.7833, P=0.0372) with a trend in Mf3s (r=-0.704, P=0.0775) (Figure 5B). When the ratio of Mf1:Mf3 was compared with the *Prevotella*: *Roseburia* ratio, the Pearson correlation coefficient was r=0.924 (P=0.0029) (Figure S4b). A similar significant association was found in the Mf1:Mf3 ratio in the ascending colon (r=0.8594, P=0.0132) (Figure S4b). The *Prevotella*: *Roseburia* ratio was also positively associated with CD103+ CD11c+ cells in the duodenum (r=0.8119, P=0.0266) (Figure 5C) and ascending colonic (r=0.9077, P=0.0047) (Figure S4c) lamina propria. Finally, the duodenum viral load was also associated with the *Prevotella*: *Roseburia* ratio (r=-0.7565, P=0.0183) (Figure 5D). A similar non-significant trend was seen in the ascending colon (r=-0.6104, P=0.0809) (Figure S4d). This analysis indicates that increased *Prevotella* and reduced *Roseburia*, two key features of HIV/SIV-associated dysbiosis, are associated with myeloid cell turnover in the duodenum. Further, this dysbiosis was also associated with gut tissue viral loads.

Discussion

Recent interest in determining the mechanism of vedolizumab action has offered new avenues for understanding HIV/SIV

FIGURE 5
Anti-$\alpha_4\beta_7$ therapy is associated with a reduction in the *Prevotella*: *Roseburia* ratio. **(A)** The ratio of *Prevotella*: *Roseburia* was calculated and normalized (for visualization and comparison) for the acute infection dysbiosis timepoint (Day 14) for longitudinal fecal samples utilized for 16S rRNA sequencing. Linear regression was performed with this ratio (not normalized) on Day 161 for **(B)** the duodenal lamina propria macrophage maturity phenotypes, **(C)** CD103+ CD11c+ cells, and **(D)** tissue viral loads.

pathogenesis. Contrary to results from earlier studies, clinical samples and murine models of DSS-induced colitis showed an association with an increase in infiltrating monocytes and a decrease in mature macrophages (40). Additionally, β7-integrin-expressing monocyte infiltration exacerbates DSS-induced colitis in RAG2 mice, which lack mature lymphoid cells, emphasizing the role of monocytes, not lymphocytes, in colitis development in these models (32). Mature lamina propria macrophages express reduced CD14 and have a reduced pro-inflammatory response to lipopolysaccharide stimulation from the microbiome (28, 41). However, during IBD, an influx of peripheral CD14+ monocytes and newly-differentiated M1 macrophages capable of microbial pattern recognition enter this niche and release pro-inflammatory cytokines (42). This signaling results in a self-perpetuating cycle of pro-inflammatory macrophage infiltration. These infiltrating monocytes and pro-inflammatory M1 macrophages in the lamina propria are thought to contribute to barrier dysfunction in IBD thought to be secondary to dysfunction of tight junction proteins and the induction of epithelial apoptosis (42). Unlike infliximab, vedolizumab is associated with significant changes in macrophage populations in human patients with CD or UC, not in lymphocyte populations, including a shift from M1 phenotype dominance to M2 (17). Infliximab, though, by blocking TNF-α, may additionally allow a similar increase in anti-inflammatory macrophage phenotypes (43).

SIV infection is associated with a shift in pro-inflammatory monocyte infiltration to gut tissues replacing mature tissue macrophages, similar to the data from IBD patients (44, 45). In RMs, the frequencies of CD163+ macrophages increased four-fold during SIV infection associated with progression to AIDS (46). Additionally, SIV infection is associated with a shift from mature CD163+CD206+ macrophages in the lamina propria to immature CD163+CD206- macrophages, with changes primarily in the small intestine (19). By applying a different flow cytometry gating approach, we provide evidence for lower percent of Mf1 and higher Mf3 macrophages following anti-$\alpha_4\beta_7$ therapy that is initiated during acute infection, compared with controls. Further, we found that it is the small intestinal lamina propria on which anti-$\alpha_4\beta_7$ mAb seems to exert the most influence, given the fact that we found differences only in CD206 co-localization with CD163 in the colon using microscopy, but not by flow cytometry, and no differences in the muscularis externa macrophage populations. Additionally, it has been hypothesized that longer-lived macrophages are more likely to serve as viral reservoirs in the tissue (19). Although we did not measure this directly, we found tissue viral loads to be closely associated with Mf3s and negatively associated with Mf1s in both tissues. This was confirmed based on CD206 co-localization with CD163, which also correlates with viral loads in the duodenum. Despite this increase in tissue viral load, it should be noted that natural hosts of SIV experience chronic viremia without progressing to AIDS (47). Results of a recent study in which whole gut tissue transcriptomic data were

compared between African green monkeys (AGMs) (*Chlorocebus* spp.; non-progressing natural hosts of SIV) and disease-susceptible RMs following SIV infection demonstrated a significantly higher expression of M2 wound-healing macrophage associated genes in AGMs following SIV infection compared with RM gut tissue which had an increase in pro-inflammatory gene expression (48). Whether anti-$\alpha_4\beta_7$ facilitates a similar switch to wound-healing remains an additional possibility requiring further investigation.

While anti-$\alpha_4\beta_7$ alone modulates monocyte trafficking associated with an increase in pro-inflammatory Mf1 macrophages to the lamina propria, we also found the frequency of multiple myeloid cell subsets to be related to the *Prevotella*: *Roseburia* ratio. HIV and SIV are each associated with acute and chronic dysbiosis, even during cART. Prominently, the overall ratio of Bacteroidetes : Firmicutes increases, primarily due to the rise in *Prevotella* at the expense of several Firmicute taxa, a pattern consistent across populations (25, 26, 37, 38, 49, 50). Whether these findings are independent of sexual behavior remains unclear, but similar trends are seen in children and SIV-infected non-human primates (37, 38, 49, 50). In addition to being characteristic of HIV-associated dysbiosis, *Prevotella* has been associated with CD4+ and CD8+ T cell activation in HIV-infected adults (51). *Prevotella* is also negatively related to CD4+ counts in perinatally-infected children and positively associated with plasma IP-10 and soluble CD14 levels, the latter implicating a role in monocyte and/or macrophage activation (37). Further, the inclusion of *Prevotella* in specific pathogen-free mice leads to a significant decrease in the relative abundance of the Firmicutes such as Lachnospiraceae and Ruminococcaceae spp. and exacerbates mucosal inflammation and disease progression in models of colitis in mice suggesting the expansion of *Prevotella* alone may be exacerbating HIV-associated inflammation and dysbiosis (52–54). In contrast to *Prevotella* expansion, several butyrate-producing Firmicute taxa are depleted during HIV pathogenesis, even during cART (25, 26, 37, 38). Most prominently, the relative abundance of colonic *Roseburia* is negatively correlated with plasma viral loads, CD4+ T cell activation, and markers of microbial translocation in PLWH. The colonic ratio of *Prevotella stercorea*: *Roseburia intestinalis* is closely associated with the activation of peripheral CD4+ T cells and colonic DCs, CD4+, and CD8+ T cells in PLWH (25). The short-chain fatty acid butyrate has a pleiotropic role in maintaining gut homeostasis, acting as an energy source for gut epithelial cells, a histone deacetylase inhibitor, and an agonist of GPR41, GPR43, and GPR109A (34, 55). GPR109A agonism specifically facilitates gut macrophages exposed to butyrate to establish their anti-inflammatory phenotype (56). Further, *ex vivo* colonic macrophages cultured with butyrate are imprinted with anti-microbial activity without a concurrent increase in tissue damage (57). Additionally, butyrate-producing bacteria like *Roseburia* have previously been linked to vedolizumab efficacy in IBDs (35), but the results presented herein, we

submit, are the first to implicate the microbiome's role, and the ratio of *Prevotella: Roseburia* specifically, to be closely associated with macrophage phenotype and function following anti-$\alpha_4\beta_7$ therapy during SIV infection.

The data presented herein represents a study significantly different from previous evaluations of anti-$\alpha_4\beta_7$ that offers insight into its potential mechanism during SIV infection. Because of these differences, tissue viral loads, in particular, were higher in anti-$\alpha_4\beta_7$-treated animals compared to controls, while previous reports found the opposite (8, 58). There are several possible reasons for this discrepancy. Computer modeling has shown that anti-$\alpha_4\beta_7$ mAb's facilitation of viral clearance was a prominent mechanism in two of the eight animals in the 2016 study (27). Additionally, the macaques in the current study were depleted of CD8+ T and NK cells by administering an anti-CD8α mAb. When performed in the original 2016 cohort following prolonged virologic control, anti-CD8α administration led to rapid viremia (27). Because CD8+ cells have been demonstrated to play a role in anti-$\alpha_4\beta_7$ efficacy, these findings provide a potential reason for differences in gut tissue viral loads. Finally, diet significantly impacts immune function and viral reservoir (59, 60). Specifically, butyrate produced from the fermentation of dietary fiber can, among other functions, act as an HDAC inhibitor (34). Although HDAC inhibitors have been explored in HIV cure strategies, these studies rarely characterized tissue macrophage reservoirs resistant to cytolysis (61). Whether this mechanism or the immune modulation induced by anti-$\alpha_4\beta_7$ infusions contributed to differences warrants further investigation, as previously suggested (27). Further investigation is needed to confirm changes in the colon with a larger number of animals to see if the macrophage immunophenotypic differences in the duodenum and its correlation with the *Prevotella : Roseburia* ratio is also present in this tissue.
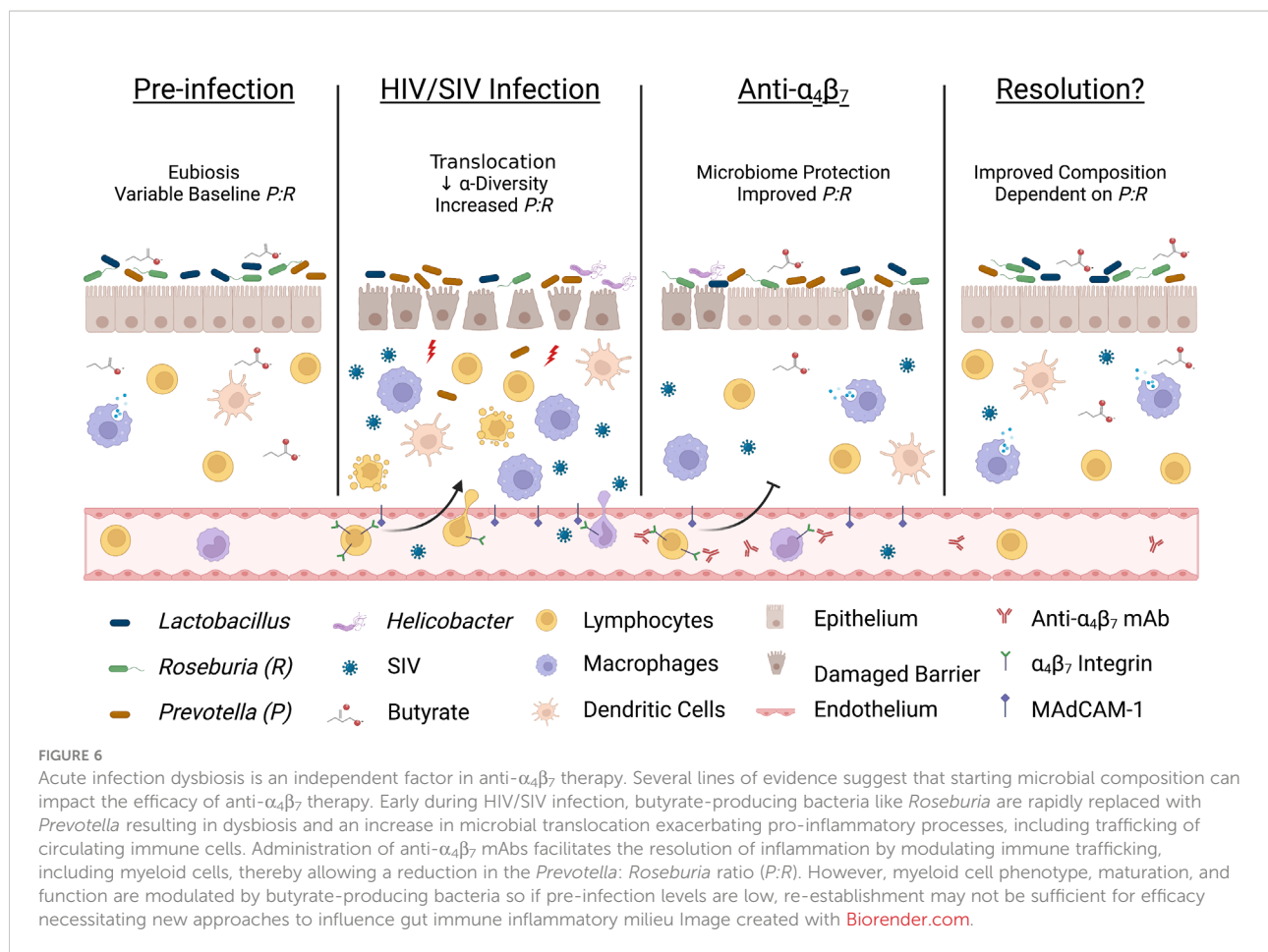
In addition to immunologic differences, the differences in virus tropism may have also played a role in gut tissue viral load compared with previous studies. Recently, the expression of HIV restriction factor SERINC5 was shown to increase in the process of macrophage differentiation (62). When incorporated into HIV virions, SERINC5 inhibits fusion with target cells, but Nef expression reduces SERINC5 incorporation. Further, HIV-1 ΔNef has a reduced ability to infect mature macrophages. In comparison, infection of HIV-1 ΔNef was non-statistically increased in monocytes (62). If anti-$\alpha_4\beta_7$ reduces the abundance of monocytes, the lack of functional Nef at infection in the original study may partially explain differences in gut viral loads (8). This is particularly true if longer-lived, mature macrophages serve as reservoirs (19). Even without the nef-stop mutation, SIVmac239 has comparatively lower macrophage tropism than dual tropic SIVmac251 used in this study (63, 64). Additionally, it is known that $\alpha_4\beta_7$ becomes incorporated into SIV/HIV, and when comparisons of $\alpha_4\beta_7$ integrin incorporations were made in diverse HIV and SIV strains, it was found that SIVmac251 had

the highest levels of incorporation of the 14 total viruses examined (65). Such $\alpha_4\beta_7$ incorporation into virions has been attributed to increased trafficking to the gut facilitating trans-infection of cells close to MADCAM-1 (65). Regardless of the SIV viral stock used, rapid SIV diversification *in vivo* means that reduced myeloid turnover likely enhances the viral reservoir, thereby increasing tissue viral loads when control monkeys replace macrophages with uninfected monocytes during cART suppression. However, it should be noted that earlier anti-$\alpha_4\beta_7$ administration studies have been inconsistent, with some unable to replicate viral control and others showing increased time to viral rebound when co-administered with neutralizing antibodies (11, 12, 66, 67). While macrophage turnover is rapid during SIV infection, complete suppression may be necessary prior to anti-$\alpha_4\beta_7$ therapy to reduce tissue viral loads (19). Future studies need to determine if macrophage turnover and therefore reduced maturity during cART can help limit the tissue macrophage reservoir, thereby explaining discrepancies between our study and previous findings. If true, a delay in initiating anti-$\alpha_4\beta_7$ administration may improve tissue virologic outcomes.

Although our findings are statistically significant, the interpretation of our data has limitations beyond differences in study design compared with previous similar studies. First, the study utilized for this analysis was designed to test a different hypothesis and was meant to be preliminary. Because of this design, the sample size was small, and two samples were missing for our flow cytometry analysis, thus reducing their statistical power. Next, cART was also interrupted several weeks before necropsy, making translation to IBDs or cART-suppressed PLWH impossible since ongoing viral replication may influence macrophage maturity. Unlike previous studies determining macrophage and monocyte turnover during SIV infection, we did not utilize BrdU to track recently divided cells and instead relied on newly developed flow cytometry techniques and previously validated microscopic markers to determine gut macrophage maturity (19, 28). Finally, the microbiome analysis was performed on fecal samples instead of gut tissue, which are usually only partially correlated (68, 69). Additionally, several factors, including local viral replication, may modulate the microbiome, further complicating interpretation. Therefore, future additional studies incorporating these limitations may address the precise mechanisms behind these observations, and further studies are warranted in this direction.

Conclusions

The *in vivo* administration of a primatized anti-$\alpha_4\beta_7$ mAbs during SIV suppression has yielded inconsistent results on virologic control suggesting the involvement of a complex mechanism and possible co-factors that may be responsible for differential efficacy. First, we found that increased macrophage maturity phenotypes were associated with tissue viral loads, a difference from earlier studies that administered anti-$\alpha_4\beta_7$ after

FIGURE 6

Acute infection dysbiosis is an independent factor in anti-$\alpha_4\beta_7$ therapy. Several lines of evidence suggest that starting microbial composition can impact the efficacy of anti-$\alpha_4\beta_7$ therapy. Early during HIV/SIV infection, butyrate-producing bacteria like *Roseburia* are rapidly replaced with *Prevotella* resulting in dysbiosis and an increase in microbial translocation exacerbating pro-inflammatory processes, including trafficking of circulating immune cells. Administration of anti-$\alpha_4\beta_7$ mAbs facilitates the resolution of inflammation by modulating immune trafficking, including myeloid cells, thereby allowing a reduction in the *Prevotella: Roseburia* ratio (*P:R*). However, myeloid cell phenotype, maturation, and function are modulated by butyrate-producing bacteria so if pre-infection levels are low, re-establishment may not be sufficient for efficacy necessitating new approaches to influence gut immune inflammatory milieu Image created with Biorender.com.

infection. This may indicate that the timing of anti-$\alpha_4\beta_7$ administration with regard to tissue viral suppression is an essential determinant of efficacy. Second, we found that dysbiosis markers are associated with the relative impact of anti-$\alpha_4\beta_7$ on macrophage maturity. Low dietary fiber consumption in humans is associated with reduced butyrate production and increased risk of IBD (59, 60), and the relative abundance of BPB has been shown to impact the efficacy of vedolizumab in humans (35). Based on the data presented herein, we propose that important shifts in microbiome composition during HIV/SIV infections like increases in *Prevotella* spp. and depletion of BPB like *Roseburia* spp. may be key independent factors in anti-$\alpha_4\beta_7$-treated SIV-infected macaques (Figure 6). Future studies aiming to modulate gut immune function in HIV/SIV should include assays like 16S rRNA sequencing of colon/fecal samples to characterize microbiome dynamics at baseline, acute dysbiosis, during, and following therapeutic intervention. Further, factors impacting gut microbial diversity and composition, such as animal source, age, co-housing, antibiotic use, and diet, should be considered when interpreting such study results.

Data availability statement

The original contributions presented in the study are included in the article/Supplementary Material. FASTQ files generated during 16S rRNA sequencing are deposited in the NCBI Sequence Read Archive with the BioProject accession number PRJNA870961.

Ethics statement

The animal study was reviewed and approved by University of Nebraska Medical Center Institutional Animal Care and Use Committee (IACUC).

Author contributions

SB designed the study and SJ, LK, participated in research design. SJ and LK performed animal protocols. OO designed antibody panel and ran flow cytometer. SJ performed flow cytometry analysis. SJ and

Conflict of interest

The authors declare that the research was conducted in the absence of any commercial or financial relationships that could be construed as a potential conflict of interest.

Publisher's note

All claims expressed in this article are solely those of the authors and do not necessarily represent those of their affiliated organizations, or those of the publisher, the editors and the reviewers. Any product that may be evaluated in this article, or claim that may be made by its manufacturer, is not guaranteed or endorsed by the publisher.

Supplementary material

The Supplementary Material for this article can be found online at: https://www.frontiersin.org/articles/10.3389/fimmu.2022.1001727/full#supplementary-material

References

1. Mudd JC, Brenchley JM. Gut mucosal barrier dysfunction, microbial dysbiosis, and their role in HIV-1 disease progression. *J Infect Dis* (2016) 214 (suppl_2):S58–66. doi: 10.1093/infdis/jiw258

2. Alzahrani J, Hussain T, Simar D, Palchaudhuri R, Abdel-Mohsen M, Crowe SM, et al. Inflammatory and immunometabolic consequences of gut dysfunction in HIV: Parallels with IBD and implications for reservoir persistence and non-AIDS comorbidities. *EBioMedicine* (2019) 46:522–31. doi: 10.1016/j.ebiom.2019.07.027

3. Serlin MH, Dieterich D. Gastrointestinal disorders in HIV. *Global HIV/AIDS Med* (2008), 251–60. doi: 10.1016/B978-1-4160-2882-6.50027-7

4. Zhu Z, Zhao R, Hu Y. Symptom clusters in people living with HIV: A systematic review. *J Pain Symptom Manage* (2019) 58(1):115–33. doi: 10.1016/j.jpainsymman.2019.03.018

5. McLean LP, Shea-Donohue T, Cross RK. Vedolizumab for the treatment of ulcerative colitis and crohn's disease. *Immunotherapy* (2012) 4(9):883–98. doi: 10.2217/imt.12.85

6. Byrareddy SN, Sidell N, Arthos J, Cicala C, Zhao C, Little DM, et al. Species-specific differences in the expression and regulation of $\alpha_4\beta_7$ integrin in various nonhuman primates. *J Immunol* (2015) 194(12):5968–79. doi: 10.4049/jimmunol.1402866.

7. Pereira LE, Onlamoon N, Wang X, Wang R, Li J, Reimann KA, et al. Preliminary *in vivo* efficacy studies of a recombinant rhesus anti-$\alpha_4\beta_7$ monoclonal antibody. *Cell Immunol* (2009) 259(2):165–76. doi: 10.1016/j.cellimm.2009.06.012

8. Byrareddy Siddappa N, Arthos J, Cicala C, Villinger F, Ortiz Kristina T, Little D, et al. Sustained virologic control in SIV+ macaques after antiretroviral and $\alpha_4\beta_7$ antibody therapy. *Science* (2016) 354(6309):197–202. doi: 10.1126/science.aag1276.

9. Byrareddy SN, Kallam B, Arthos J, Cicala C, Nawaz F, Hiatt J, et al. Targeting $\alpha_4\beta_7$ integrin reduces mucosal transmission of simian immunodeficiency virus and protects gut-associated lymphoid tissue from infection. *Nat Med* (2014) 20 (12):1397–400. doi: 10.1038/nm.3715

10. Uzzan M, Tokuyama M, Rosenstein AK, Tomescu C, SahBandar IN, Ko HM, et al. Anti-$\alpha_4\beta_7$ therapy targets lymphoid aggregates in the gastrointestinal tract of HIV-1–infected individuals. *Sci Trans Med* (2018) 10(461):eaau4711. doi: 10.1126/scitranslmed.aau4711

11. Abbink P, Mercado NB, Nkolola JP, Peterson RL, Tuyishime H, McMahan K, et al. Lack of therapeutic efficacy of an antibody to $\alpha_4\beta_7$ in SIVmac251-infected rhesus macaques. *Science* (2019) 365(6457):1029–33. doi: 10.1126/science.aaw8562

12. Di Mascio M, Lifson JD, Srinivasula S, Kim I, DeGrange P, Keele BF, et al. Evaluation of an antibody to $\alpha_4\beta_7$ in the control of SIVmac239-nef-stop infection. *Science* (2019) 365(6457):1025–9. doi: 10.1126/science.aav6695

13. Ziani W, Shao J, Fang A, Connolly PJ, Wang X, Veazey RS, et al. Mucosal integrin $\alpha_4\beta_7$ blockade fails to reduce the seeding and size of viral reservoirs in SIV-infected rhesus macaques. *FASEB J* (2021) 35(2):e21282. doi: 10.1096/fj.202002235R

14. Sneller MC, Clarridge KE, Seamon C, Shi V, Zorawski MD, Justement JS, et al. An open-label phase 1 clinical trial of the anti-$\alpha_4\beta_7$ monoclonal antibody vedolizumab in HIV-infected individuals. *Sci Transl Med* (2019) 11(509):eaax3447. doi: 10.1126/scitranslmed.aax3447

15. Frank I, Cigoli M, Arif MS, Fahlberg MD, Maldonado S, Calenda G, et al. Blocking $\alpha_4\beta_7$ integrin delays viral rebound in SHIVSF162P3-infected macaques treated with anti-HIV broadly neutralizing antibodies. *Sci Trans Med* (2021) 13 (607):eabf7201. doi: 10.1126/scitranslmed.abf7201

16. Luzentales-Simpson M, Pang YCF, Zhang A, Sousa JA, Sly LM. Vedolizumab: Potential mechanisms of action for reducing pathological inflammation in inflammatory bowel diseases. *Front Cell Dev Biol* (2021) 9(120). doi: 10.3389/fcell.2021.612830

17. Zeissig S, Rosati E, Dowds CM, Aden K, Bethge J, Schulte B, et al. Vedolizumab is associated with changes in innate rather than adaptive immunity in patients with inflammatory bowel disease. *Gut* (2019) 68(1):25. doi: 10.1136/gutjnl-2018-316023

18. Takahashi N, Ardeshir A, Holder GE, Cai Y, Sugimoto C, Mori K, et al. Comparison of predictors for terminal disease progression in simian immunodeficiency virus/simian-HIV-infected rhesus macaques. *AIDS* (2021) 35 (7):1021–9. doi: 10.1097/QAD.0000000000002874

19. Takahashi N, Sugimoto C, Allers C, Alvarez X, Kim W-K, Didier ES, et al. Shifting dynamics of intestinal macrophages during simian immunodeficiency virus infection in adult rhesus macaques. *J Immunol (Baltimore Md 1950)* (2019) 202(9):2682–9. doi: 10.4049/jimmunol.1801457

20. Sanchis-Artero L, Martínez-Blanch JF, Manresa-Vera S, Cortés-Castell E, Valls-Gandia M, Iborra M, et al. Evaluation of changes in intestinal microbiota in crohn's disease patients after anti-TNF alpha treatment. *Sci Rep* (2021) 11 (1):10016. doi: 10.1038/s41598-021-88823-2

21. Clooney AG, Eckenberger J, Laserna-Mendieta E, Sexton KA, Bernstein MT, Vagianos K, et al. Ranking microbiome variance in inflammatory bowel disease: a

large longitudinal intercontinental study. *Gut* (2021) 70(3):499. doi: 10.1136/gutjnl-2020-321106

22. Sokol H, Seksik P, Furet JP, Firmesse O, Nion-Larmurier I, Beaugerie L, et al. Low counts of faecalibacterium prausnitzii in colitis microbiota. *Inflammatory Bowel Dis* (2009) 15(8):1183–9. doi: 10.1002/ibd.20903

23. Machiels K, Joossens M, Sabino J, De Preter V, Arijs I, Eeckhaut V, et al. A decrease of the butyrate-producing species Roseburia hominis and Faecalibacterium prausnitzii defines dysbiosis in patients with ulcerative colitis. *Gut* (2014) 63(8):1275–83. doi: 10.1136/gutjnl-2013-304833

24. Nie K, Ma K, Luo W, Shen Z, Yang Z, Xiao M, et al. Roseburia intestinalis: A beneficial gut organism from the discoveries in genus and species. *Front Cell Infection Microbiol* (2021) 11:757718. doi: 10.3389/fcimb.2021.757718.

25. Dillon SM, Kibbie J, Lee EJ, Guo K, Santiago ML, Austin GL, et al. Low abundance of colonic butyrate-producing bacteria in HIV infection is associated with microbial translocation and immune activation. *AIDS* (2017) 31(4):511–21. doi: 10.1097/QAD.0000000000001366

26. Crakes KR, Jiang G. Gut microbiome alterations during HIV/SIV infection: Implications for HIV cure. *Front Microbiol* (2019) 10:1104. doi: 10.3389/fmicb.2019.01104

27. Wells CR, Cao Y, Durham DP, Byrareddy SN, Ansari AA, Ruddle NH, et al. Mechanistic basis of post-treatment control of SIV after anti-$\alpha_4\beta_7$ antibody therapy. *PloS Comput Biol* (2021) 17(6):e1009031. doi: 10.1371/journal.pcbi.1009031

28. Bujko A, Atlasy N, Landsverk OJB, Richter L, Yaqub S, Horneland R, et al. Transcriptional and functional profiling defines human small intestinal macrophage subsets. *J Exp Med* (2017) 215(2):441–58. doi: 10.1084/jem.20170057

29. Acharya A, Olwenyi Omalla A, Thurman M, Pandey K, Morsey Brenda M, Lamberty B, et al. Chronic morphine administration differentially modulates viral reservoirs in a simian immunodeficiency virus SIVmac251-infected rhesus macaque model. *J Virol* (2020) 95(5):e01657–20. doi: 10.1128/JVI.01657-20

30. Dyavar SR, Ye Z, Byrareddy SN, Scarsi KK, Winchester LC, Weinhold JA, et al. Normalization of cell associated antiretroviral drug concentrations with a novel RPP30 droplet digital PCR assay. *Sci Rep* (2018) 8(1):3626. doi: 10.1038/s41598-018-21882-0

31. Bolte S, CordeliÈRes FP. A guided tour into subcellular colocalization analysis in light microscopy. *J Microscopy* (2006) 224(3):213–32. doi: 10.1111/j.1365-2818.2006.01706.x

32. Schippers A, Muschaweck M, Clahsen T, Tautorat S, Grieb L, Tenbrock K, et al. β7-integrin exacerbates experimental DSS-induced colitis in mice by directing inflammatory monocytes into the colon. *Mucosal Immunol* (2016) 9(2):527–38. doi: 10.1038/mi.2015.82

33. Clahsen T, Pabst O, Tenbrock K, Schippers A, Wagner N. Localization of dendritic cells in the gut epithelium requires MAdCAM-1. *Clin Immunol* (2015) 156(1):74–84. doi: 10.1016/j.clim.2014.11.005

34. Wang J, Chen W-D, Wang Y-D. The relationship between gut microbiota and inflammatory diseases: The role of macrophages. *Front Microbiol* (1065) 2020:11:1065. doi: 10.3389/fmicb.2020.01065

35. Ananthakrishnan AN, Luo C, Yajnik V, Khalili H, Garber JJ, Stevens BW, et al. Gut microbiome function predicts response to anti-integrin biologic therapy in inflammatory bowel diseases. *Cell Host Microbe* (2017) 21(5):603–10.e3. doi: 10.1016/j.chom.2017.04.010

36. Groves HT, Higham SL, Moffatt MF, Cox MJ, Tregoning JS. Respiratory viral infection alters the gut microbiota by inducing inappetence. *mBio* (2020) 11(1):e03236–19. doi: 10.1128/mBio.03236-19

37. Kaur U, Shet A, Rajnala N, Gopalan B, Moar P, Himanshu D, et al. High abundance of genus prevotella in the gut of perinatally HIV-infected children is associated with IP-10 levels despite therapy. *Sci Rep* (2018) 8(1):17679. doi: 10.1038/s41598-018-35877-4

38. Siddiqui S, Bao D, Doyle-Meyers L, Dufour J, Wu Y, Liu Y-Z, et al. Alterations of the gut bacterial microbiota in rhesus macaques with SIV infection and on short- or long-term antiretroviral therapy. *Sci Rep* (2020) 10(1):19056. doi: 10.1038/s41598-020-76145-8

39. Mutlu EA, Keshavarzian A, Losurdo J, Swanson G, Siewe B, Forsyth C, et al. A compositional look at the human gastrointestinal microbiome and immune activation parameters in HIV infected subjects. *PloS Pathog* (2014) 10(2):e1003829.

40. Jones G-R, Bain CC, Fenton TM, Kelly A, Brown SL, Ivens AC, et al. Dynamics of colon monocyte and macrophage activation during colitis. *Front Immunol* (2018) 9(2764). doi: 10.3389/fimmu.2018.02764

41. Smith PD, Smythies LE, Mosteller-Barnum M, Sibley DA, Russell MW, Merger M, et al. Intestinal macrophages lack CD14 and CD89 and consequently are down-regulated for LPS- and IgA-mediated activities. *J Immunol* (2001) 167(5):2651. doi: 10.4049/jimmunol.167.5.2651

42. Lissner D, Schumann M, Batra A, Kredel L-I, Kühl AA, Erben U, et al. Monocyte and M1 macrophage-induced barrier defect contributes to chronic intestinal inflammation in IBD. *Inflammatory bowel Dis* (2015) 21(6):1297–305. doi: 10.1097/MIB.0000000000000384

43. Koelink PJ, Bloemendaal FM, Li B, Westera L, Vogels EWM, van Roest M, et al. Anti-TNF therapy in IBD exerts its therapeutic effect through macrophage IL-10 signalling. *Gut* (2020) 69(6):1053. doi: 10.1136/gutjnl-2019-318264

44. Kamada N, Hisamatsu T, Okamoto S, Chinen H, Kobayashi T, Sato T, et al. Unique CD14 intestinal macrophages contribute to the pathogenesis of crohn disease *via* IL-23/IFN-gamma axis. *J Clin Invest* (2008) 118(6):2269–80. doi: 10.1172/JCI34610

45. Gren ST, Grip O. Role of monocytes and intestinal macrophages in crohn's disease and ulcerative colitis. *Inflammation Bowel Dis* (2016) 22(8):1992–8. doi: 10.1097/MIB.0000000000000824

46. Swan ZD, Wonderlich ER, Barratt-Boyes SM. Macrophage accumulation in gut mucosa differentiates AIDS from chronic SIV infection in rhesus macaques. *Eur J Immunol* (2016) 46(2):446–54. doi: 10.1002/eji.201545738

47. Chahroudi A, Bosinger Steven E, Vanderford Thomas H, Paiardini M, Silvestri G. Natural SIV hosts: Showing AIDS the door. *Science* (2012) 335(6073):1188–93. doi: 10.1126/science.1217550

48. Barrenas F, Raehtz K, Xu C, Law L, Green RR, Silvestri G, et al. Macrophage-associated wound healing contributes to African green monkey SIV pathogenesis control. *Nat Commun* (2019) 10(1):5101. doi: 10.1038/s41467-019-12987-9

49. Vujkovic-Cvijin I, Sortino O, Verheij E, Sklar J, Wit FW, Kootstra NA, et al. HIV-Associated gut dysbiosis is independent of sexual practice and correlates with noncommunicable diseases. *Nat Commun* (2020) 11(1):2448. doi: 10.1038/s41467-020-16222-8

50. Noguera-Julian M, Rocafort M, Guillén Y, Rivera J, Casadellà M, Nowak P, et al. Gut microbiota linked to sexual preference and HIV infection. *EBioMedicine* (2016) 5:135–46. doi: 10.1016/j.ebiom.2016.01.032

51. Dillon SM, Lee EJ, Kotter CV, Austin GL, Dong Z, Hecht DK, et al. An altered intestinal mucosal microbiome in HIV-1 infection is associated with mucosal and systemic immune activation and endotoxemia. *Mucosal Immunol* (2014) 7(4):983–94. doi: 10.1038/mi.2013.116

52. Iljazovic A, Roy U, Gálvez E, Lesker T, Zhao B, Gronow A, et al. Perturbation of the gut microbiome by prevotella spp. enhances host susceptibility to mucosal inflammation. *Mucosal Immunol* (2020) 14:1–12. doi: 10.1038/s41385-020-0296-4

53. Chen Y, Lin H, Cole M, Morris A, Martinson J, McKay H, et al. Signature changes in gut microbiome are associated with increased susceptibility to HIV-1 infection in MSM. *Microbiome* (2021) 9(1):237. doi: 10.1186/s40168-021-01168-w.

54. Sui Y, Dzutsev A, Venzon D, Frey B, Thovarai V, Trinchieri G, et al. Influence of gut microbiome on mucosal immune activation and SHIV viral transmission in naive macaques. *Mucosal Immunol* (2018) 11(4):1219–29. doi: 10.1038/s41385-018-0029-0.

55. Salvi PS, Cowles RA. Butyrate and the intestinal epithelium: Modulation of proliferation and inflammation in homeostasis and disease. *Cells* (2021) 10(7):1775. doi: 10.3390/cells10071775.

56. Singh N, Gurav A, Sivaprakasam S, Brady E, Padia R, Shi H, et al. Activation of Gpr109a, receptor for niacin and the commensal metabolite butyrate, suppresses colonic inflammation and carcinogenesis. *Immunity* (2014) 40(1):128–39. doi: 10.1016/j.immuni.2013.12.007

57. Schulthess J, Pandey S, Capitani M, Rue-Albrecht KC, Arnold I, Franchini F, et al. The short chain fatty acid butyrate imprints an antimicrobial program in macrophages. *Immunity* (2019) 50(2):432–45.e7. doi: 10.1016/j.immuni.2018.12.018

58. Santangelo PJ, Cicala C, Byrareddy SN, Ortiz KT, Little D, Lindsay KE, et al. Early treatment of SIV+ macaques with an $\alpha_4\beta_7$ mAb alters virus distribution and preserves CD4+ T cells in later stages of infection. *Mucosal Immunol* (2018) 11(3):932–46. doi: 10.1038/mi.2017.112

59. Milajerdi A, Ebrahimi-Daryani N, Dieleman LA, Larijani B, Esmaillzadeh A. Association of dietary fiber, fruit, and vegetable consumption with risk of inflammatory bowel disease: A systematic review and meta-analysis. *Adv Nutr* (2021) 12(3):735–43. doi: 10.1093/advances/nmaa145

60. Pituch-Zdanowska A, Banaszkiewicz A, Albrecht P. The role of dietary fibre in inflammatory bowel disease. *Prz Gastroenterol* (2015) 10(3):135–41. doi: 10.5114/pg.2015.52753

61. Clayton KL, Collins DR, Lengieza J, Ghebremichael M, Dotiwala F, Lieberman J, et al. Resistance of HIV-infected macrophages to CD8+ T lymphocyte–mediated killing drives activation of the immune system. *Nat Immunol* (2018) 19(5):475–86. doi: 10.1038/s41590-018-0085-3

62. Zutz A, Schölz C, Schneider S, Pierini V, Münchhoff M, Sutter K, et al. SERINC5 is an unconventional HIV restriction factor that is upregulated during myeloid cell differentiation. *J Innate Immun* (2020) 12(5):399–409. doi: 10.1159/000504888

63. Yen P-J, Mefford ME, Hoxie JA, Williams KC, Desrosiers RC, Gabuzda D. Identification and characterization of a macrophage-tropic SIV envelope

glycoprotein variant in blood from early infection in SIVmac251-infected macaques. *Virology* (2014) 458-459:53–68. doi: 10.1016/j.virol.2014.03.024

64. Villinger F. *In-vivo* use of SIVmac239 with a reversing stop codon in the SIV nef gene. *AIDS* (2020) 34(3):487. doi: 10.1097/QAD.0000000000002429

65. Guzzo C, Ichikawa D, Park C, Phillips D, Liu Q, Zhang P, et al. Virion incorporation of integrin $\alpha_4\beta_7$ facilitates HIV-1 infection and intestinal homing. *Sci Immunol* (2017) 2(11):eaam7341. doi: 10.1126/sciimmunol.aam7341

66. Frank I, Cigoli M, Arif MS, Fahlberg MD, Maldonado S, Calenda G, et al. Blocking $\alpha_4\beta_7$ integrin delays viral rebound in SHIVSF162P3-infected macaques treated with anti-HIV broadly neutralizing antibodies. *Sci Transl Med* (2021) 13 (607):eabf7201. doi: 10.1126/scitranslmed.abf7201

67. Iwamoto N, Mason RD, Song K, Gorman J, Welles HC, Arthos J, et al. Blocking $\alpha_4\beta_7$ integrin binding to SIV does not improve virologic control. *Science* (2019) 365(6457):1033–6. doi: 10.1126/science.aaw7765

68. Zmora N, Zilberman-Schapira G, Suez J, Mor U, Dori-Bachash M, Bashiardes S, et al. Personalized gut mucosal colonization resistance to empiric probiotics is associated with unique host and microbiome features. *Cell* (2018) 174 (6):1388–405.e21. doi: 10.1016/j.cell.2018.08.041

69. Ringel Y, Maharshak N, Ringel-Kulka T, Wolber EA, Sartor RB, Carroll IM. High throughput sequencing reveals distinct microbial populations within the mucosal and luminal niches in healthy individuals. *Gut Microbes* (2015) 6(3):173–81. doi: 10.1080/19490976.2015.1044711